GNSS Multipath Failures Modes Analysis for Airport Surface Operations

Leslie Montloin, Laurent Azoulai, Anaïs Martineau, Carl Milner, Christophe Macabiau

GNSS multipath failures modes analysis for airport surface operations

Leslie MONTLOIN, Laurent AZOULAI, *Airbus, Toulouse, France*
Anaïs MARTINEAU, Carl MILNER, Christophe MACABIAU, *ENAC Telecom Lab, Toulouse, France*

BIOGRAPHIES

Leslie MONTLOIN has a Master degree in electronic from the ENAC (French National School for Civil Aviation). Since 2011, she is a PhD student in the Signal Processing and Navigation Research Group (SIGNAV) of ENAC in Toulouse, France. The PhD project is in collaboration with the radio navigation group of Airbus. She is currently working on multipath modeling for taxi and parking operations.

Laurent AZOULAI graduated in 1996 of Institut Supérieur de l'Electronique de Paris as an engineer specialized in automatic systems. He is GNSS-Landing Systems Technical Expert within Airbus His activities focus on Approach and Landing and the use of GNSS in Communication, Navigation and Surveillance Airbus aircraft systems. He is involved in standardization activities dealing with GBAS Cat 2/3, GPS/Galileo and SBAS for which he is co-chairman of RTCA SC-159 SBAS Working Group.

Dr. Anaïs MARTINEAU graduated in 2005 as an electronics engineer from the Ecole Nationale de l'Aviation Civile (ENAC) in Toulouse, France. Since 2005, she has been working at the signal processing lab of the ENAC where she carries out research on integrity monitoring techniques. She received her Ph.D. in 2008 from the University of Toulouse.

Dr. Carl MILNER is an Assistant Professor within the Telecom Lab at the Ecole Nationale Aviation Civile. He has a Master's degree in Mathematics from the University of Warwick, a PhD in Geomatics from Imperial College London and has completed the graduate trainee programme at the European Space Agency. His research interests include GNSS augmentation systems, integrity monitoring, air navigation and applied mathematics.

Dr. Christophe MACABIAU graduated as an electronics engineer in 1992 from the ENAC in Toulouse, France. Since 1994, he has been working on the application of satellite navigation techniques to civil aviation. He received his PhD in 1997 and has been in charge of the signal processing lab of ENAC since 2000.

ABSTRACT

Global Navigation Satellite System (GNSS) is currently used in civil aviation to provide aircraft with position and velocity estimates from en-route to Precision Approach (PA) operations. Extending the use of GNSS to automatic taxi and parking remains a challenge. Indeed, during surface operations, GNSS pseudo range measurements suffer from higher multipath errors than whilst in flight because of signal reflections from the aircraft structure, and from additional sources of multipath that are the airport surface and obstacles surrounding the airborne antenna [2]. The standardized multipath error model [8] used by integrity monitoring algorithms during in-flight operations is not valid for surface operations. Current integrity monitoring algorithms are thus not designed to protect users from the effects of multipath during surface operations. Hence it is necessary to develop an integrity monitoring algorithm designed to properly detect multipath ranging errors and protect users from the effects of multipath during surface operations. Several steps are needed to set up such an algorithm.

The first step [4] was to model the raw code ranging errors due to multipath from:

- the aircraft structure and the airport surface,
- the aircraft structure, the airport surface, and obstacles surrounding the airborne antenna,

in both static and dynamic conditions.

The second step, which is the main objective of this paper, is to define multipath faults modes that may potentially affect GNSS pseudo range measurements during surface operations.
Firstly, the navigation algorithm considered for the faults modes identification is presented. The algorithm is a tight-coupling GNSS+Inertial Navigation System (INS) Kalman filter. The accuracy performances of the navigation algorithm in both static and dynamic configurations are obtained by simulations. Next, performances are compared to the accuracy requirements that are demanded for the control function. This function will be used to perform automatic taxi and parking operations.
Secondly, analytical models of the horizontal position error at the Kalman filter output are provided in both

static and dynamic conditions. These models are adapted to taxi and parking operations. The impact of multipath ranging errors on the horizontal position error is underlined. In the static case, the multipath ranging errors are deterministic multipath ranging biases. Ranging biases induce a deterministic horizontal position error. Parameters of the navigation algorithm influencing the multipath-induced deterministic positioning error are presented and their influences are discussed. In the dynamic case, the multipath ranging errors are modeled as the sum of a deterministic bias and a stochastic error that follows a centered Gaussian distribution. The multipath stochastic errors induce an inflation of the variance of the horizontal position error. Parameters influencing the variance of the horizontal position error are presented and their influences are discussed.
Thirdly, the concept of multipath faults is defined. A practical methodology aiming to identify single and double multipath faults is proposed. The methodology requires implementing and simulating the horizontal position error models presented herein. Based on this methodology, the static single and double multipath faults for the control function during taxi operations are identified. Next, the dynamic single multipath faults for the control function during taxi and parking on the apron operations are identified.

INTRODUCTION

GNSS is currently used in civil aviation to provide aircraft with position and velocity estimates from en-route to PA operations. GNSS is also currently used during surface operations for the position awareness (also known as routing [15]) function. This function aims to display the airport map and the routes to follow on navigation displays. The challenge for the incoming years is to extend the use of GNSSs to automatic surface operations. This will require the future airport navigation systems to combine guidance and control functions [15]. The guidance function will provide indications to the pilot to follow the assigned route [1]. The control function will allow the pilot to drive in all weather conditions using steering indications [1].
Compared to the position awareness function, the guidance and control functions require high performance (meter level) on the aircraft positioning service in terms of accuracy and integrity [1]. Integrity is a measure of the trust which can be placed in the correctness of the information provided by the total system. It includes the ability of a system to provide timely and valid warnings when the system must not be used for the intended operation [7].
One of the main issues in extending the use of GNSSs to these stringent functions is multipath. Multipath is the reception of echo replicas of the desired signal by the GNSS airborne antenna. For in-flight operations, the structure of the aircraft itself is the dominant source of multipath error. A multipath ranging errors model has been standardized and is currently used GNSS integrity monitoring algorithms for in-flight operations [8]. However, during taxi and parking operations, additional sources of multipath errors may affect the pseudo-range measurements [2]:
- the airport surface, which can be modeled in airport environments by tar or grass to represent taxiways,
- obstacles on the airport surface surrounding the GNSS airborne antenna such as aircrafts and buildings.

These additional sources of multipath result in two main consequences. Firstly, multipath replicas are one of the dominant contributors of error for surface operations. Multipath errors on raw code pseudo range measurements may reach few m [4]. This may lead to multipath errors in the horizontal positioning domain of up to few dm, which is significant with respect to the required meter level accuracy. Hence multipath may significantly degrade the accuracy performance of the GNSS-based navigation systems during airport surface operations. Secondly, the standardized multipath error model is not valid for surface operations. Current integrity monitoring algorithms are thus not designed to protect users from the effects of multipath during surface operations.
Considering these issues, the main objective of our project is to propose an integrity monitoring algorithm capable to support guidance and control functions during surface operations and designed to protect users from the effects of multipath. The design of such an algorithm requires an understanding of the multipath faults modes as well as their probability of occurrence [16]. In this project, “multipath faults” are qualitatively defined using the GPS integrity fault definition provided in [16]: a multipath fault is a multipath ranging error inconsistent with the nominal error distribution due to a fault condition and which can lead to a position error larger than the maximum tolerable error for a given pair function/operation. The proposed integrity monitoring algorithm will be capable to detect multipath faults with a probability of missed detection that depends on the probabilities of occurrence of the multipath faults and on the integrity requirements.

In order to achieve the main objective presented herein, several steps are needed. The first step aimed to provide multipath ranging errors models adapted to surface operations [4]. The second step objectives constitute the main goals of this paper that are:
- to propose a GNSS-based navigation system capable to support the accuracy requirements for surface operations,
- to identify the multipath faults for control function during taxi and parking on the apron operations.

This paper is organized as follows:
- The **first section** defines the operations and functions targeted in this publication as well as the operational

performance required by these operations/functions. It also provides the general architecture of the GNSS-based navigation system considered for the rest of the paper. Finally, this part introduces the main assumptions made on the GNSS measurements used in the navigation system and the main notations used in the paper.

- The **second section** provides a brief summary of the static and dynamic multipath ranging errors models that are adapted to surface operations and developed in [4]. Next, for each static and dynamic configuration, position errors models adapted to taxi and parking on the apron operations are proposed. These errors models are specific to the navigation algorithm presented in the first section, that is to say the Kalman filter.
- The **third section** provides the simulation results. Firstly, the simulations conditions are exposed. Secondly, the simulation-based methodology to assess the accuracy performance of the GNSS-based navigation system described in the first section is presented. Simulations results are compared to the accuracy requirements proposed in [1] for the control function during taxi and parking on the apron operations. Thirdly, the paper explains how the position error models established in the second section are used in simulations to identify the multipath faults. Multipath faults are then identified for the control function during taxi and parking on the apron operations.
- Finally, the main results derived in this paper and future works are presented in the **conclusion**.

I. SYSTEM MODEL

This section aims to provide the general architecture of the positioning algorithm used in the paper and to introduce the notations that will be used.

This publication focuses on two types of surfaces operations: taxi and parking on the apron. The taxi on the taxiway operation begins when the aircraft exits the runway or the high speed taxiway [17]. It ends when the aircraft enters the apron area and begins the parking on the apron operation. The apron area is defined as the area intended to accommodate aircraft for purposes of loading or unloading passengers away from airport terminals [15]. The apron operation ends when the aircraft enters the gate region and moves on taxilanes [17]. In addition, only control function is considered in this paper. The control function will allow the pilot to drive in all weather conditions using steering indications [1].
The positioning system and the integrity monitoring system must be chosen in order to support the operational requirements in terms of accuracy and integrity for the control function during taxi and parking on the apron. These requirements are provided in Table 1. In this Table, HAL stands for Horizontal Alert Limit.

Operation	Accuracy 95% bound requirement	Integrity requirement		
		HAL	Integrity risk	Time to Alert
Taxi	1m	4,5m	1e-9/op	1s
Parking on the apron	1m	7,5m	1e-7/op	1s

Table 1: Operational requirements on the aircraft positioning system for control function [1]

In order to meet the meter level accuracy and integrity operational requirements indicated in Table 1, few solutions could be envisaged. Firstly, the use of corrections broadcasted by Satellite Based Augmentation System (SBAS) satellites could help to reduce the errors affecting GNSS pseudo range measurements. However, the visibility of SBAS satellites may be degraded in airport environments. Secondly, the use of multi constellation and multi frequency Ground Based Augmentation Systems (GBASs) could also help to reduce the positioning error. Multi constellation multi frequency Aircraft Based Augmentation Systems (ABASs) based on the hybridization of GNSS measurements with external sensors is a third solution to meet the meter level accuracy and integrity operational requirements. Since this solution will most likely be available before the operation of multi constellation and multi frequency GBAS systems in airport environments, a multi sensors GNSS+INS tight coupling positioning algorithm is considered in this paper and is represented in Figure 1.

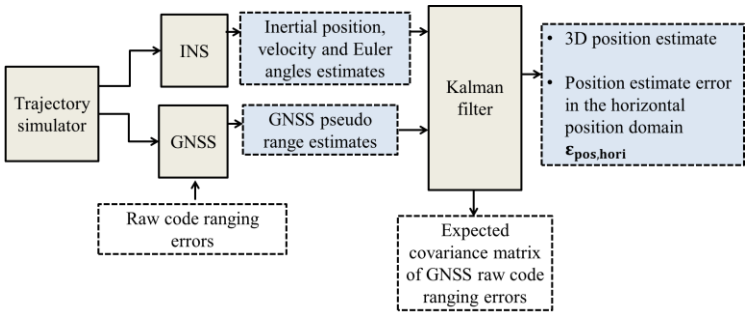

Figure 1: Architecture of the position estimate error simulator

In this paper, a double constellation GPS+Galileo is considered. Note that the 24 GPS and 27 Galileo satellites are considered to be static during a surface operation that lasts few tens of s up to few min. Indeed, a preliminary analysis shows that the angular variation of the satellite elevation and azimuth angles does not exceed few tenths of degrees during a time period of few min. These angular variations are neglected in this paper. Each GPS and Galileo satellite is assumed to broadcast GPS L1C and GPS L5 signals. Each Galileo satellite is assumed to broadcast Galileo E1C and Galileo E5 signals.

GPSL1C/L5 and GalileoE1/E5a raw (or unsmoothed) code iono free pseudo range measurements are used to estimate the aircraft position. 4 types of errors affect GNSS raw code pseudo range measurements that are:

- The **multipath** error. The raw code multipath ranging error is denoted as $\varepsilon_{\text{code multipath}}$ in Figure 1,
- The residual **satellite clock and ephemeris** errors after correction by Aircraft Based Augmentation System (ABAS) standardized correction models,
- The residual **tropospheric** error after correction of the tropospheric delay by ABAS standardized correction models,
- The GNSS airborne **receiver noise** error.

The INS estimates the position, velocity and attitude angles of the aircraft based on measurements made by the INS sensors, namely the gyroscopes and the accelerometers. INS sensors measurements are affected by errors. Both GNSS and INS sensors measurements errors induce errors in the horizontal position estimated at the Kalman filter output. Horizontal position error is denoted as $\boldsymbol{\varepsilon_{pos,hori}} = \begin{bmatrix} \varepsilon_{\text{pos,North}} \\ \varepsilon_{\text{pos,East}} \end{bmatrix}$ in Figure 1. The next section aims to propose models of $\boldsymbol{\varepsilon_{pos,hori}}$ adapted to airport surface operations.

II. POSITION ERROR MODELS

Several publications underline the impact of aircraft dynamics on the multipath ranging errors affecting the raw code pseudo range estimates [2] [3]. Hence, a previous publication proposes separate raw code multipath ranging error models for both static and dynamic configurations [4]. Since the position error models at the Kalman filter output depends on the multipath ranging error models, separate position error models for both static and dynamic configurations are provided in this publication.

II.1. Static Case

II.1.1. Multipath ranging error models

The multipath ranging error models adapted to the static case and developed in [4] are briefly presented below. Let's assume that the aircraft is static in the airport as represented in Figure 2.

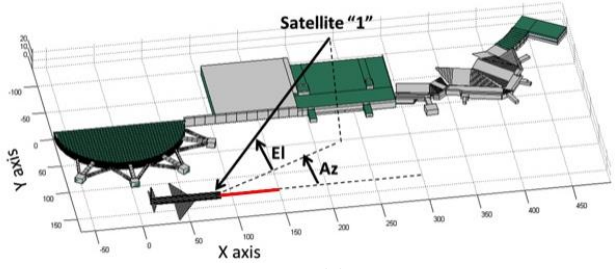

Case (a)

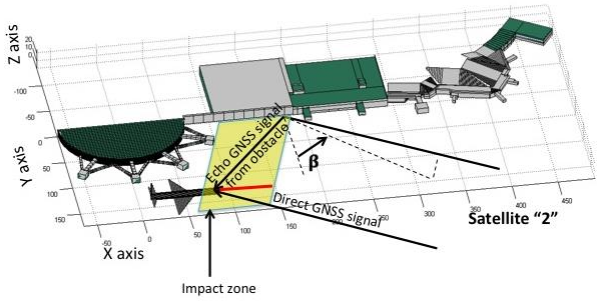

Case (b)

Figure 2: static aircraft in an airport

Considering that the multipath sources and the satellite "j" are static, and considering that the Delay Locked Loop (DLL) is in steady state, the raw code multipath ranging error that affects the pseudo range measurement between the satellite "j" and the airborne antenna remains constant in the time domain:

$$\varepsilon_{\text{code multipath,l}} = b \; \forall t_l, \text{DLL in steady state} \qquad \text{Eq.1}$$

where:

- b is the DLL output code multipath ranging error in steady state.

The amplitude of b highly depends on the multipath sources that induce the error on the pseudo range measurement between a satellite "j" and the airborne antenna. More precisely, 2 cases can be distinguished and are illustrated in Figure 2:

- Case (a): the pseudo range measurement is affected by multipath from the airport surface and the aircraft structure,
- Case (b) : the pseudo range measurement is affected by multipath from the airport surface the aircraft structure and obstacles surrounding the airborne antenna.

The value of b related to both cases are indicated in Table 2.

Case	Value of b
Case (a)	$b_{A/C+ground}(El, Az)$
Case (b)	$b_{A/C+ground+obs}$

Table 2: raw code multipath ranging errors models in static configuration

Case (a)

From Table 2, the raw code multipath ranging error due to multipath from the airport surface and from the aircraft structure (Case (a)) is a bias $b_{A/C+ground}(El, Az)$ in the DLL steady state. $b_{A/C+ground}(El, Az)$ mainly depends on the satellite elevation angle El. It also depends on the relative orientation of the aircraft fuselage with respect to the satellite. This angle is denoted as Az in Figure 2 (a).

The values of $b_{A/C+ground}$ for a wide range of elevation angles have been simulated on GPS L1C, GPS L5, Galileo E1C and Galileo E5a measurements with the deterministic multipath ranging error simulator described in [2]. Values of $b_{A/C+ground}$ are plotted in Figure 3 for dual frequency measurements GPSL1C/L5 and GalileoE1/E5a and for $Az = 0°$.

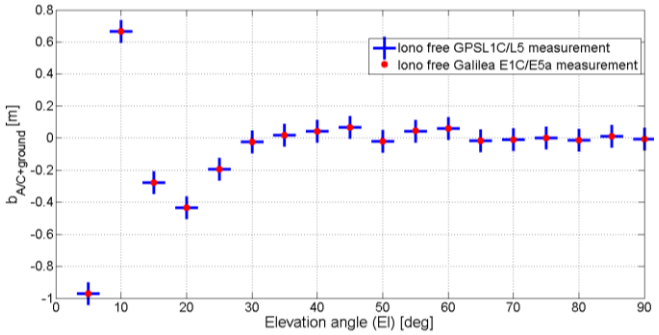

Figure 3: $b_{A/C+ground}$ as a function of the elevation angle, $Az = 0°$

Case (b)

From Table 2, the raw code multipath ranging error due to multipath from the airport surface, the aircraft structure and obstacle(s) (Case (b)) is a bias $b_{A/C+ground+obs}$ in the DLL steady state. $b_{A/C+ground+obs}$ mainly depends on:

- The relative position of the airborne antenna with respect to the obstacle(s),
- The obstacle(s) characteristics (sizes, materials and shapes),
- The satellite elevation angle (El),
- The orientation of the façade of the obstacle(s) with respect to the direction of propagation of the incoming GNSS signal (β).

Note that El, Az and β are illustrated in Figure 2.

II.1.2. Position error model

The goal of this subsection is to model the horizontal position estimate error at the Kalman filter output when the aircraft is static in the airport. The GNSS raw code pseudo range measurement error vector at time t_l is given by:

$$\mathbf{w_l} = \underbrace{\begin{bmatrix} v_{sat\ 1,l} \\ \vdots \\ v_{sat\ N,l} \end{bmatrix}}_{\mathbf{v_l}} + \underbrace{\begin{bmatrix} \varepsilon_{sat\ 1,code\ multipath,l} \\ \vdots \\ \varepsilon_{sat\ N,code\ multipath,l} \end{bmatrix}}_{\mathbf{b_l}} \qquad \text{Eq.2}$$

where:

- N is the number of GNSS raw code pseudo range measurements used in the Kalman filter to estimate the aircraft position at time t_l,
- $\mathbf{v_l}$ is the GNSS raw code pseudo range measurement error vector due to the receiver noise ranging error, the residual satellite clock error and ephemeris errors and the tropospheric delay estimation error,
- $\mathbf{b_l}$ is a biases vector that represents the GNSS raw code multipath ranging errors vector. $\mathbf{b_l}$ is developed in Section **II.1.1.**

Note that, in Eq.2, the total ranging error is assumed to be the sum of the ranging errors due to all error contributors. Eq.2 is true if we consider that the tracking loops can be approximated by linear models. This assumption is valid in our application since the ranging errors standard deviations of the different contributors of errors are sufficiently low regarding the parameters of the tracking loops.

From **APPENDIX**, $\boldsymbol{\varepsilon_{pos,hori}}$ at time t_l follows a Gaussian distribution characterized by a deterministic vector denoted as $E[\boldsymbol{\varepsilon_{pos,hori,l}}]\ (2 \times 1)$ and by a covariance matrix denoted as $\mathrm{cov}[\boldsymbol{\varepsilon_{pos,hori,l}}]\ (2 \times 2)$:

$$\boldsymbol{\varepsilon_{pos,hori,l}} \sim N\left(E[\boldsymbol{\varepsilon_{pos,hori,l}}], \mathrm{cov}[\boldsymbol{\varepsilon_{pos,hori,l}}]\right) \qquad \text{Eq.3}$$

where:

- $\mathrm{cov}[\boldsymbol{\varepsilon_{pos,hori,l}}] = \mathbf{C_{sat\&eph,tropo,noise}}$ is the horizontal position estimate error covariance matrix that would have been obtained if $\mathbf{w_l} = \mathbf{v_l}$,
- $E[\boldsymbol{\varepsilon_{pos,hori,l}}] = \left((\mathbf{I} - \mathbf{K_l} \times \mathbf{H_l})(\mathbf{F_{l-1}} \times E[\mathbf{X_{l-1}} - \widehat{\mathbf{X}}^{+}_{l-1}]) \quad - \mathbf{K_l} \times \mathbf{b_l}\right)_{1:2}$
- **K, H** and **F** are the Kalman matrices presented in **APPENDIX, X** is the Kalman state vector and $\widehat{\mathbf{X}}^{+}$ is the a posteriori state vector estimated by the Kalman filter,
- $E[\boldsymbol{\varepsilon_{pos,hori,0}}] = \mathbf{0}_{2\times1}$,
- $(\mathbf{A})_{1:2}$ represents the first 2 lines of vector A,
- $(\mathbf{X_l})_{1:1}$ represents the position error in the North direction at time t_l,
- $(\mathbf{X_l})_{2:2}$ represents the position error in the east direction at time t_l.

From Eq. 3, the multipath ranging biases vector $\mathbf{b_l}$ induces a horizontal deterministic position error $E[\boldsymbol{\varepsilon_{pos,hori,l}}]$ which is illustrated as follows. Let's assume that, during the simulation, the satellite constellation is considered as fixed. During the period of the simulation, $N = 13$ GNSS raw code pseudo range measurements are used to estimate the static aircraft position. Indeed, preliminary simulations have shown that the number of visible satellites in Toulouse Blagnac airport, France, depends on the instant of the day and varies between 10 and 15 satellites considering a double constellation GPS+Galileo. The Kalman filter is assumed to be in steady state during the time period of the simulation.
For $t_l < t_K$ the 13 GNSS measurements are affected by multipath from the airport surface and from the aircraft structure.

From $t_l = t_K$, the GNSS signal received from satellite "2" is suddenly affected by an additional multipath from one obstacle of the airport until the end of the simulation. This results in a raw code multipath ranging bias on the pseudo range from satellite "2" denoted as $b_{sat\,2,A/C+ground+obs,l}$. Hence, from Section **II.1.1.**, $\mathbf{b_l}$ is given by:

$$\forall\, t_l < t_K, \mathbf{b_l} = \begin{bmatrix} b_{A/C+ground}(El_{sat\,1}, Az_{sat\,1}) \\ \vdots \\ b_{A/C+ground}(El_{sat\,13}, Az_{sat\,13}) \end{bmatrix} \quad \text{Eq.4}$$

$$\forall\, t_l \geq t_K, \mathbf{b_l} = \begin{bmatrix} b_{A/C+ground}(El_{sat\,1}, Az_{sat\,1}) \\ b_{sat\,2,A/C+ground+obs,l} \\ \vdots \\ b_{A/C+ground}(El_{sat\,13}, Az_{sat\,13}) \end{bmatrix} \quad \text{Eq.5}$$

Figure 4 represents the evolution of the multipath bias on the raw code pseudo range measurement between satellite "2" and the antenna (black line). In this graph, the transient period of the DLL is neglected and the multipath bias on the 2nd GNSS measurement is assumed to converge immediately to $b_{sat\,2,A/C+ground+obs}$ at $t_l = t_K$. The effect of the DLL transient state on the deterministic position error is not detailed in this paper and is left as future work. The North (blue line) and East (red line) components of the deterministic position estimate error vector $E[\boldsymbol{\varepsilon}_{\mathbf{pos,hori,l}}]$ in the presence of the multipath biases vector $\mathbf{b_l}$ are computed based on Eq. 3 and plotted in Figure 4 as well. Note that the Kalman matrices **K, H** and **F** needed to compute $E[\boldsymbol{\varepsilon}_{\mathbf{pos,hori,l}}]$ have been obtained by simulations using the position error simulator represented in Figure 1.

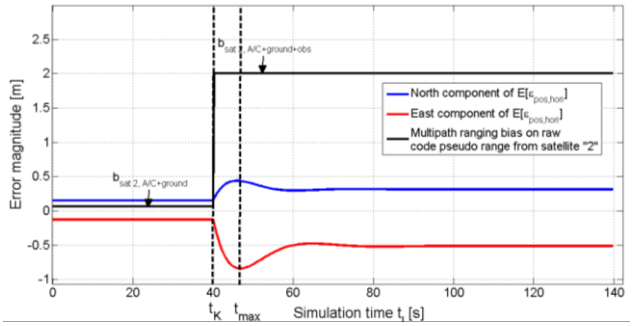

Figure 4: Deterministic position error in the North and East directions

As depicted in Figure 4, the deterministic position error in the North and East directions present few oscillations in the time domain and converge to final time-constant values. The amplitude of the oscillations can reach 2 times the value of the final time-constant value.

The shape of the position error is interpreted as follows. From Eq.3, $E[\varepsilon_{pos,hori,l}]$ can be considered as the response of an equivalent filter to the raw code pseudo range biases vector b_l. The coefficients of the equivalent filter depend on the Kalman matrices **K**, **H** and **F**. Since GNSS satellites and aircraft are considered as static, since the expected covariance matrix of the raw code pseudo range measurement errors is constant during the simulation, and since the Kalman filter is in steady state, the coefficients of the equivalent filter remain roughly constant. Hence, the deterministic position estimate errors in the North and East directions converge to time-constant values.

Moreover, the transient period of the Kalman filter, defined in this subsection as the time period between t_K and the time epoch corresponding to the stabilization of the deterministic position errors in the time domain, lasts roughly 30s. This transient time mainly depends on the expected values of the raw code pseudo range measurement errors standard deviations that are given to the Kalman filter. In our simulation, these values are low (few dm). The Kalman filter mainly "relies on" the measurement model, the Kalman gain is thus relatively high, and the transient period is thus relatively long.

II.2. Dynamic Case

II.2.1. Multipath ranging error models

The multipath ranging error models adapted to the dynamic case and developed in [4] are briefly presented below. Let's assume that the aircraft performs a straight line trajectory with a constant speed in the airport as represented in Figure 2 (red line).

The values of $\varepsilon_{code\,multipath,l}$ highly depends on the multipath sources that induce the error on the pseudo range measurement between a satellite "j" and the airborne antenna along the trajectory. As for the static case, 2 cases can be distinguished and are illustrated in Figure 2:

- Case (a): the pseudo range measurement is affected by multipath from the airport surface and the aircraft structure,
- Case (b) : the pseudo range measurement is affected by multipath from the airport surface the aircraft structure and obstacles surrounding the airborne antenna.

The model of $\varepsilon_{code\,multipath,l}$ along the trajectory related to both cases are indicated in Table 3.

Case	Model of $\varepsilon_{\text{code multipath,l}}$
Case (a)	$\varepsilon_{\text{code multipath,l}}$ remains constant since both elevation angle (El) and fuselage orientation (Az) remain roughly constant during a straight line trajectory. $\varepsilon_{\text{code multipath,l}} = b_{A/C+ground}(El, Az)$
Case (b)	$\varepsilon_{\text{code multipath,l}}$ presents high variations along the trajectory and is modeled by a stationary non centered Gaussian law $\varepsilon_{\text{code multipath,l}} \sim N(b_{A/C+ground+obs}, \sigma_{A/C+ground+obs})$

Table 3: raw code multipath ranging errors models in dynamic configuration

Case (a)
From Table 3, the raw code multipath ranging error due to multipath from the airport surface and from the aircraft structure (Case (a)) is a constant bias $b_{A/C+ground}(El, Az)$ along the trajectory. Details about the value of $b_{A/C+ground}(El, Az)$ are provided in Section **II.1.1.**

Case (b)
The raw code multipath ranging error due to multipath from the airport surface, the aircraft structure and obstacle(s) (Case (b)) presents small scales (dm level) strong amplitude variations (up to m level amplitude) along the trajectory. This is due to the high spatial variations of the multipath ranging errors in the airport area where the field scattered by the illuminated façade of the obstacle(s) is concentrated [4]. This area is called "impact zone". Hence $\varepsilon_{\text{code multipath,l}}$ can be considered as a stochastic error. More specifically, [4] shows that $\varepsilon_{\text{code multipath,l}}$ along a straight line trajectory in an impact zone follows a stationary Gaussian distribution characterized by a mean $b_{A/C+ground+obs}$ and a standard deviation $\sigma_{A/C+ground+obs}$. $b_{A/C+ground+obs}$ and $\sigma_{A/C+ground+obs}$ mainly depend on:

- The obstacle(s) characteristics (sizes, materials and shapes),
- The satellite elevation angle (El),
- The orientation of the façade of the obstacle(s) with respect to the direction of propagation of the incoming GNSS signal (β).

Note that El, Az and β are illustrated in Figure 2. Due to the effect of the DLL on the raw code ranging errors, the errors $\varepsilon_{\text{code multipath,l}}$ are time-correlated along the trajectory. In this paper, $\varepsilon_{\text{code multipath,l}}$ is assumed to follow a first-order Gauss-Markov process characterized by an auto-correlation time of the inverse of the DLL bandwidth, that is to say $T = 1s$.

II.2.2. Position error model

The goal of this subsection is to model the horizontal position estimate error at the Kalman filter output when the aircraft performs a constant-speed straight line trajectory in the airport in the airport. The GNSS raw code pseudo range measurement error vector at time t_l is given by:

$$\mathbf{w_l} = \underbrace{\begin{bmatrix} v_{\text{sat 1,l}} \\ \vdots \\ v_{\text{sat N,l}} \end{bmatrix}}_{\mathbf{v_l}} + \begin{bmatrix} \varepsilon_{\text{sat 1,code multipath,l}} \\ \vdots \\ \varepsilon_{\text{sat N,code multipath,l}} \end{bmatrix} \qquad \text{Eq.6}$$

where:

- N and $\mathbf{v_l}$ are defined in Section **II.1.2.**
- $\varepsilon_{\text{sat j,code multipath,l}} = b_{A/C+ground}(El_{\text{sat j}}, Az_{\text{sat j}})$ is a deterministic error if the GNSS pseudo range measurement from satellite "j" to the airborne antenna is affected by multipath from the airport surface and the aircraft structure,
- $\varepsilon_{\text{sat j,code multipath,l}} = b_{\text{sat j,A/C+ground+obs}} + x_{\text{sat j,l}}$ where $b_{\text{sat j,A/C+ground+obs}}$ is the deterministic part of $\varepsilon_{\text{sat j,code multipath,l}}$ and $x_{\text{sat j,l}} \sim N(0, \sigma_{\text{sat j,A/C+ground+obs}})$ is the stochastic part of $\varepsilon_{\text{sat j,code multipath,l}}$ if the pseudo range measurement is also affected by multipath from obstacle(s).

Hence:

$$\mathbf{w_l} = \mathbf{v_l} + \mathbf{b_l} + \mathbf{x_l}$$

where:

- $\mathbf{b_l}$ is a biases vector that represents the deterministic part of the GNSS raw code multipath ranging errors vector,
- $\mathbf{x_l}$ represents the stochastic part of the GNSS raw code multipath ranging errors vector.

From **APPENDIX**, $\boldsymbol{\varepsilon_{pos,hori}}$ at time t_l follows a Gaussian distribution:

$$\boldsymbol{\varepsilon_{pos,hori,l}} \sim N(E[\boldsymbol{\varepsilon_{pos,hori,l}}], \text{cov}[\boldsymbol{\varepsilon_{pos,hori,l}}]) \qquad \text{Eq.7}$$

where:

- $E[\boldsymbol{\varepsilon_{pos,hori,l}}]$ is the deterministic position error vector induced by the pseudo range biases vector $\mathbf{b_l}$. Details about $E[\boldsymbol{\varepsilon_{pos,hori,l}}]$ are provided in Section **II.1.2.**
- $\text{cov}[\boldsymbol{\varepsilon_{pos,hori,l}}] = \mathbf{C_{sat\&eph,tropo,noise}} + \mathbf{C_{mp,l}}$
- $\mathbf{C_{sat\&eph,tropo,noise}}$ is defined in in Section **II.1.2**
- $\mathbf{C_{mp}}$ represents the inflation of the covariance of the position error due to the presence of stochastic multipath ranging errors:

$$\mathbf{C_{mp,l}} = \left(\mathbf{B_l C_{mp,l-1} B_l}^{\mathbf{T}} + \mathbf{K_l R_{mp,l}\, K_l}^{\mathbf{T}} - 2\mathbf{B_l} E\left[\Delta \mathbf{X_{l-1,mp}} \times \mathbf{x_{l-1}}^{\mathbf{T}}\right] \mathbf{CORR_l}^{\mathbf{T}} \mathbf{K_l}^{\mathbf{T}}\right)_{1:2,1:2}$$

- $\mathbf{R_{mp,l}}$ is the multipath ranging error covariance matrix at time t_l,
- $\mathbf{CORR_l}$ contains the correlation times of the stochastic multipath ranging errors at time t_l,
- $\mathbf{B_l}$, $\Delta\mathbf{X_{l,mp}}$, $\mathbf{K_l}$ are defined in **APPENDIX**,
- $\mathbf{x_l}$ is the stochastic part of the multipath ranging error vector at time t_l,
- $\mathbf{C_{mp,0}} = \mathbf{0_{2\times 2}}$, $E\left[\Delta \mathbf{X_{0,mp}} \times \mathbf{x_0}^{\mathbf{T}}\right] = \mathbf{0}$,
- $E\left[\Delta \mathbf{X_{l,mp}} \times \mathbf{x_l}^{\mathbf{T}}\right]$ can be computed by recurrence from **APPENDIX**.

Note that Eq.6 and Eq.7 have been derived assuming that the tracking loops can be approximated by linear models. As explained in Section **II.1.2**, this assumption is valid in our application.

An important remark is that, in Eq.3 and Eq.7, a model of the true behavior of the position error is proposed assuming a sub-optimal Kalman filter. In other words, the filter does not contain the exact model of the measurement process. Indeed, the Kalman gain is calculated using a measurement error covariance matrix that does not contain the model of multipath errors.

From Eq. 7, the stochastic multipath ranging vector $\mathbf{x_l}$ induces an inflation of the horizontal position error covariance matrix $\mathbf{C_{mp}}$ which is illustrated as follows. Let's consider an aircraft performing a straight line trajectory in an airport. During the simulation, a constant number of ranging measurements (13) are used to estimate the aircraft position. The Kalman filter is assumed to be in steady state.

- For $t_l < t_K$ 13 GNSS measurements are affected by multipath from the airport surface and from the aircraft structure.
- From $t_l = t_K$, the GNSS signal received from satellite "2" is suddenly affected by additional multipath from one obstacle of the airport until the end of the simulation. This results in a raw code multipath ranging error on the pseudo range from satellite "2" $\varepsilon_{\text{sat 2,code multipath,l}} = b_{\text{sat 2,A/C+ground+obs}} + x_{\text{sat2,l}}$, where $x_{\text{sat2,l}} \sim N\left(0, \sigma_{\text{sat 2,A/C+ground+obs}}\right)$:

$$\forall\, t_l < t_K, \mathbf{x_l} = \begin{bmatrix} 0 \\ \vdots \\ 0 \end{bmatrix} \text{ and } \forall\, t_l \geq t_K, \mathbf{x_l} = \begin{bmatrix} 0 \\ x_{\text{sat2,l}} \\ \vdots \\ 0 \end{bmatrix} \quad \text{Eq.8}$$

Figure 5 represents the evolution of the multipath error standard deviation on the raw code pseudo range measurement between satellite "2" and the antenna (black line). The North and East components of the position estimate error covariance matrix $\text{cov}\left[\boldsymbol{\varepsilon}_{\mathbf{pos,hori,l}}\right]$ are computed based on Equation 7. The square root of the covariance in the North (blue line) and East (red line) directions are plotted in Figure 5. Note that the Kalman matrices **K, B** and $\mathbf{C_{sat\&eph,tropo,noise}}$ needed to compute $\text{cov}\left[\boldsymbol{\varepsilon}_{\mathbf{pos,hori,l}}\right]$ have been obtained by simulations using the position error simulator represented in Figure 1.

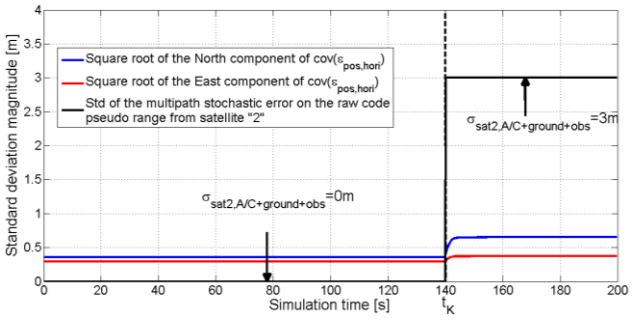

Figure 5: Position error standard deviations in the North and East directions

Note that, as for the deterministic position errors, the position error standard deviations in both North and East directions become constant after a transient state that follows the apparition of the stochastic ranging error on the pseudo range between satellite "2" and the airborne receiver. An interpretation of this behavior is proposed in Section **II.1.2.**

III. SIMULATIONS RESULTS

In Section II, the impact of raw code multipath ranging errors on the position error has been assessed. Multipath ranging errors have been classified as follows:

- Errors due to multipath from the aircraft structure and the airport surface. These errors are called "nominal multipath errors" in the following.
- Errors due to multipath from the aircraft structure, from the airport surface and from obstacles. They may affect temporally one or several pseudo range measurements, regarding the relative location of the satellites, the aircraft and the obstacles of the airport. These errors are called "abnormal multipath errors" or errors "inconsistent with the nominal error distribution" in the following.

The main goals of this Section are to assess the accuracy performance of the positioning algorithm provided in Figure 1 under nominal conditions and to identify the multipath faults modes that may occur during surface operations.

Both accuracy performance analysis and faults modes identification have been performed assuming particular models for the nominal errors affecting the inertial sensors (gyroscopes and accelerometers) measurements

and the GNSS raw code pseudo range measurements. These errors models are presented in the next subsection.

III.1. Simulations conditions

III.1.1. Inertial sensors measurements errors

The main errors that affect gyroscopes and accelerometers measurements are listed as follows [5]:

- The Gaussian gyroscope/accelerometer measurement noise η_{IMU},
- The gyroscope/accelerometer bias $k_{0,IMU}$,
- The gyroscope/accelerometer scale factor $k_{1,IMU}$,
- The gyroscope/accelerometer misalignment misa.

The measured absolute non-gravitational acceleration / angular velocity of the aircraft expressed in the mobile frame at time t_l can be written as [6]:

$$x_{meas,l} = \eta_{IMU,l} + k_{0,IMU,l} + misa.\left(I_{3\times3} + k_{1,IMU}\right)x_{true,l} \quad \text{Eq.9}$$

where:

- $misa = \sin\begin{bmatrix} \frac{\pi}{2} - w_\theta & -w'_\psi & w_\varphi{}' \\ w'_\psi & \frac{\pi}{2} - w_\varphi & -w'_\theta \\ -w'_\varphi & w'_\theta & \frac{\pi}{2} - w_\psi \end{bmatrix}$

The values of the parameters describing the errors terms are provided in Table 4. These values are typical values used in civil aviation. In Table 4, "Std" stands for standard deviation.

Error	**Value of the parameter describing the error**	
	Gyroscope	Accelerometer
$\eta_{IMU,l}$	Std: 8.08×10^{-10}rad. s^{-1}	Std: 9.81×10^{-4}m. s^{-2}
$k_{0,IMU,l}$	1st order Gauss-Markov process Std: 4.85×10^{-8}rad. s^{-1} Autocorrelation time: 1500s	1st order Gauss-Markov process Std: 9.81×10^{-5}m. s^{-2} Autocorrelation time: 3000s
$k_{1,IMU}$	Chosen uniformly in $[-5 \times 10^{-6}\ ;\ +5 \times 10^{-6}]$	Chosen uniformly in $[-2.5 \times 10^{-5}\ ;\ +2.5 \times 10^{-5}]$
misa	$w_\theta, w'_\theta, w_\varphi, w'_\varphi, w_\psi, w'_\psi$ chosen uniformly in $[-5 \times 10^{-6}\ ;\ +5 \times 10^{-6}]$	$w_\theta, w'_\theta, w_\varphi, w'_\varphi, w_\psi, w'_\psi$ chosen uniformly in $[-5 \times 10^{-6}\ ;\ +5 \times 10^{-6}]$

Table 4 : Characteristics of the inertial sensors measurements errors models

III.1.2. GNSS measurements errors

Raw code multipath ranging error models are discussed in Section **II**. For this reason, these models are not presented in this subsection. The nominal raw code ranging errors related to the other sources of pseudo range measurement error are modelled with 1st order Gauss-Markov processes characterized by a standard deviation and by an auto-correlation time presented in Table 5.

Source of pseudo range measurement error	**Standard deviation [m]**	**Auto-correlation time [s]**
GNSS receiver noise	Derived from [11]	1 (due to a DLL bandwidth of 1Hz)
Tropospheric delay estimation error	Derived from Section J.5 of [8], [12]	1800 [8] [12]
Satellite clock error and ephemeris error	**Galileo**: 0.85 [12] **GPS**: 0.85 (expected value for future GPS constellation [13])	3600 [8] [12]

Table 5: Characteristics of the GNSS raw code pseudo range measurements errors models

Note that the standard deviation of the GNSS receiver noise ranging error depends on the C/N0 ratio of the related GNSS signal. The impact of multipath on the C/N0 ratio of each GNSS signal is left as future work. Hence, in this paper, the impact of multipath on the GNSS receiver noise error standard deviation is not taken into account.

III.2. Accuracy performance

The goal of this subsection is to obtain the accuracy performance of the positioning algorithm presented in Figure 1 under nominal conditions. The following methodology has been used. An aircraft is simulated and located in Toulouse Blagnac airport, France, during a time period of 48hr. During this time period, the satellites geometries are simulated with a time step of 15min. For each satellite geometry:

- Horizontal positioning errors $\boldsymbol{\varepsilon_{pos,hori}} = \begin{bmatrix} \varepsilon_{pos,North} \\ \varepsilon_{pos,East} \end{bmatrix}$ are computed over few hundred of seconds thanks to the positioning error simulator presented in Figure 1. The errors models presented in Section **III.1** are used in these computations. In addition, in nominal conditions, raw code pseudo range measurements are affected by multipath from the airport surface and aircraft structure described Section **II.1.1**. In order to eliminate large (dm level) multipath ranging errors that appear at low elevation angles (see Figure 3), a GPS and Galileo elevation mask angle of 15° has been chosen.
- A large number of independent horizontal positioning errors are then extracted from the computed errors.

179490 independent horizontal positioning errors have been simulated over 48hr. Data are then used to compute the percentage of the time when $|\boldsymbol{\varepsilon_{pos,hori}}|$ exceeds the 95% accuracy bound provided in Table 1. The results are shown in Table 6. Note that Table 6 shows results for both static and dynamic case since the dynamic of the system influences the performance of the positioning algorithm.

Operation	**% of the time $|\boldsymbol{\varepsilon_{pos,hori}}|$ is below the 95% accuracy bound**	
	Static aircraft	Dynamic aircraft

		(2m/s straight line trajectories)
Taxi	98.88%	98.87%
Parking on the apron	98.88%	98.87%

Table 6: Accuracy performance for the static case – control function

From Table 6, the positioning algorithm used in this paper allows meeting the accuracy requirements for the static case and for the dynamic case with a typical speed of the aircraft in the airport of 2m/s.

III.3. Multipath faults modes identification

III.3.1. Multipath faults definition

In the introductive part, a definition of the multipath faults is proposed. More specifically, it defines a multipath fault as a multipath ranging error inconsistent with the nominal error distribution that can lead to a positioning error larger than the HAL for a given function/operation. Following this definition, any multipath error due to signal reflection from the airport surface, the aircraft structure and obstacle(s) would be considered as fault. Indeed, any multipath error inconsistent with the nominal conditions and combined with nominal errors can potentially lead to a positioning error larger than the HAL with a probability that may be extremely small compared to the integrity risk. In this subsection, a criterion aiming to identify which multipath ranging errors are considered as faults is established.

The integrity risk P_{IR} provided in Table 1 is the probability of providing a position that is out of tolerance without warning the user within the time-to-alert [7]:

$$P_{IR} = P\left(\left(\left|\boldsymbol{\varepsilon}_{\mathbf{pos,hori}}\right| > \mathrm{HAL}\right) \ \&\ (\text{no detection})\right) \qquad \text{Eq.10}$$

A positioning failure occurs when $\left|\boldsymbol{\varepsilon}_{\mathbf{pos,hori}}\right| > \mathrm{HAL}$ and a Misleading Information (MI) occurs when: $\left(\left|\boldsymbol{\varepsilon}_{\mathbf{pos,hori}}\right| > \mathrm{HAL}\right)$ & (no detection)) [8]. Hence, Eq.10 becomes:

$$\begin{aligned} P_{IR} = {} & P(MI \mid H_0)P_{occ}(H_0) \\ & + \sum_j P(MI \mid \varepsilon_{\text{code multipath j}})P_{occ}(\varepsilon_{\text{code multipath j}}) \\ & + \sum_{j,k} P(MI \mid \varepsilon_{\text{code multipath j}} \text{and } \varepsilon_{\text{code multipath k}})P_{occ}(\varepsilon_{\text{code multipath j}} \text{and } \varepsilon_{\text{code multipath k}}) \\ & + P(\text{MI due to all other conditions}) \end{aligned} \qquad \text{Eq.11}$$

where:

- $P(MI \mid H_0)$ is the probability of MI knowing that the system is under nominal conditions,
- $P_{occ}(H_0)$ is the probability that the system is under nominal conditions [/op],
- $P(MI \mid \varepsilon_{\text{code multipath j}})$ is the probability of MI knowing that 1 GNSS pseudo range measurement is affected by an raw code ranging error $\varepsilon_{\text{code multipath j}}$ inconsistent with the nominal error distribution,
- $P_{occ}(\varepsilon_{\text{code multipath j}})$ is the probability of occurrence of $\varepsilon_{\text{code multipath j}}$ [/op],
- $P(MI \mid \varepsilon_{\text{code multipath j}} \text{and } \varepsilon_{\text{code multipath k}})$ is the probability of MI knowing that 2 GNSS pseudo range measurements are affected by raw code ranging errors $\varepsilon_{\text{code multipath j}}$ and $\varepsilon_{\text{code multipath k}}$ inconsistent with the nominal error distribution,
- $P_{occ}(\varepsilon_{\text{code multipath j}} \text{and } \varepsilon_{\text{code multipath k}})$ is the probability of occurrence of $\varepsilon_{\text{code multipath j}}$ and $\varepsilon_{\text{code multipath k}}$ simultaneously [/op].

Note that, in Eq.11, the probability of MI due to 3 or more simultaneous multipath ranging errors inconsistent with the nominal error distribution is neglected. Indeed, a preliminary analysis based on simulations shows that, in Toulouse Blagnac airport, this probability is not significant with respect to the allowed integrity risks. However, further investigations are needed to validate this remark. In this document, only single fault modes and double faults modes are considered and are defined below.

Let's define a single multipath fault as follows. Let's denote $\varepsilon_{\text{code multipath j}}$ a raw code multipath ranging error inconsistent with the nominal error distribution. $\varepsilon_{\text{code multipath j}}$ is a single multipath fault if the probability of MI due to the combination of $\varepsilon_{\text{code multipath j}}$ to nominal errors is non-negligible with respect to the total allowed integrity risk. In the following, we consider that the probability of MI due to a particular condition is non-negligible with respect to the integrity risk if the probability of MI is equal to or above 10% of the integrity risk. Based on these definitions, we get:

$\varepsilon_{\text{code multipath j}}$ is a fault if $\varepsilon_{\text{code multipath j}}$ may lead to:

$$P(MI \mid \varepsilon_{\text{code multipath j}})P_{occ}(\varepsilon_{\text{code multipath j}}) \geq 0.1 \times P_{IR} \qquad \text{Eq.12}$$

Since $P_{occ}(\varepsilon_{\text{code multipath j}})$ is not available at this stage of the project, let's state the following conservative assumption:

$$P_{occ}(\varepsilon_{\text{code multipath j}}) = 1/\mathrm{op} \qquad \text{Eq.13}$$

Based on this previous assumption and considering no detection algorithms to detect the positioning failures, we get: $\varepsilon_{\text{code multipath j}}$ is a fault if $\varepsilon_{\text{code multipath j}}$ can lead to:

$$P(\left|\boldsymbol{\varepsilon}_{\mathbf{pos,hori}}\right| > \mathrm{HAL} \mid \varepsilon_{\text{code multipath j}}) \geq 0.1 \times P_{IR} \qquad \text{Eq.14}$$

A similar methodology leads to:

$$\left(\varepsilon_{\text{code multipath j}}, \varepsilon_{\text{code multipath k}}\right) \text{ are double faults on 2 pseudo range measurements if they can lead to :}$$
$$P\left(\left|\boldsymbol{\varepsilon}_{\mathbf{pos,hori}}\right| > \text{HAL} \middle| \varepsilon_{\text{code multipath j}} \text{and } \varepsilon_{\text{code multipath k}}\right) \geq 0.1 \times P_{IR} \quad \text{Eq.15}$$

III.3.2.1. Static case

The raw code ranging errors $\varepsilon_{\text{code multipath}}$ inconsistent with the nominal error distribution are errors due to multipath from the airport surface, the aircraft structure and obstacle(s). These errors are constant biases in the static case and are denoted as $b_{A/C+ground+obs}$. From Eq.14, in static case, a multipath single ranging fault is a bias $b_{A/C+ground+obs,0}$ that may lead to:

$$P_{single} = P\left(\left|\varepsilon_{pos,hori}\right| > \text{HAL} \mid b_{A/C+ground+obs,0}\right) \geq 0.1 \times P_{IR} \quad \text{Eq.16}$$

Multipath double ranging faults are biases $b_{A/C+ground+obs,1}$ and $b_{A/C+ground+obs,2}$ that may lead to:

$$P_{double} = P\left(\left|\boldsymbol{\varepsilon}_{\mathbf{pos,hori}}\right| > \text{HAL} \middle| b_{A/C+ground+obs,1} \text{and } b_{A/C+ground+obs,2}\right) \geq 0.1 \times P_{IR} \quad \text{Eq.17}$$

P_{single} and P_{double} have been computed for a wide range of single biases $b_{A/C+ground+obs,0}$ and biases pairs $\left(b_{A/C+ground+obs,1}, b_{A/C+ground+obs,2}\right)$. Results are shown in Figures 6 and 7. The probabilities are provided for control function during taxi. Indeed, in this paper, we do not consider the case of a stop during the parking on the apron operation. Even if the aircraft can stop during apron operations, this situation is unlikely to happen and is not considered here.

In these computations, ranging measurements that are not affected by abnormal multipath ranging errors are affected by nominal biases due to multipath from the airport surface and from the aircraft structure (see Section **II.1**.). In order to reject large nominal biases that appear at low elevation angles, a GPS and Galileo elevation mask angle of 15° has been chosen. In addition, all raw code pseudo range measurements are affected by nominal stochastic errors detailed in Section **III.1.2**.

$\boldsymbol{\varepsilon}_{\mathbf{pos,hori}}$ is modeled by a 2 dimension Gaussian law proposed by Eq.3. The covariance matrix $\mathbf{C}_{\mathbf{sat\&eph,tropo,noise}}$ and the Kalman matrices are evaluated by simulations thanks to the simulator presented in Figure 1. The deterministic position error vector $E\left[\boldsymbol{\varepsilon}_{\mathbf{pos,hori}}\right]$ is computed based on Eq.3. P_{single} and P_{double} are finally computed from the technique detailed in [9].

Note that the probabilities of positioning failure presented in Figure 6 have been computed under specific conditions. These conditions have been chosen in order to maximize the value of P_{single} and P_{double} and thus constitutes a worst case:

- The **selected satellites geometry** is the geometry that maximizes the norm of the horizontal deterministic position error vector $\left|E\left[\boldsymbol{\varepsilon}_{\mathbf{pos,hori}}\right]\right|$ induced by nominal raw code pseudo range measurements biases due to multipath from the airport surface and aircraft structure.
- The **pseudo range measurement(s)** affected by the abnormal multipath errors are selected in a way so as to maximize the norm of the horizontal deterministic position error vector $\left|E\left[\boldsymbol{\varepsilon}_{\mathbf{pos,hori}}\right]\right|$ induced by nominal raw code pseudo range measurements biases and by the single bias $b_{A/C+ground+obs,0}$ or the biases pair $\left(b_{A/C+ground+obs,1}, b_{A/C+ground+obs,2}\right)$ [10].
- The **time instant** after apparition of the single bias $b_{A/C+ground+obs,0}$ or of the biases pair $\left(b_{A/C+ground+obs,1}, b_{A/C+ground+obs,2}\right)$ is given as follows. From Figure 4, the norm of the horizontal deterministic position error vector $\left|E\left[\boldsymbol{\varepsilon}_{\mathbf{pos,hori}}\right]\right|$ oscillates after the apparition of abnormal biases and becomes roughly constant. The time instant is selected in a way so as to maximize $\left|E\left[\boldsymbol{\varepsilon}_{\mathbf{pos,hori}}\right]\right|$. As an illustration, this time instant is denoted as t_{max} in Figure 4.

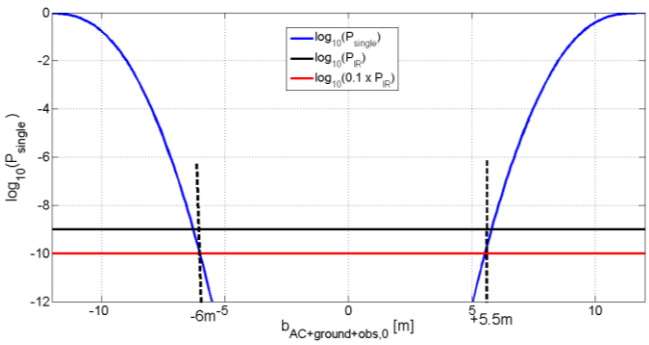

Figure 6: probability of positioning failure given a bias $b_{A/C+ground+obs,0}$ on a single pseudo range measurement – control function during taxi

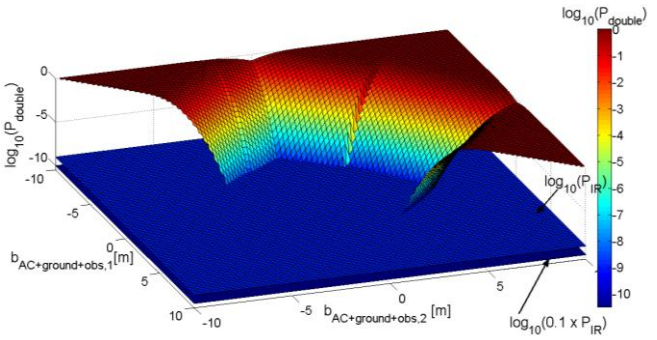

Figure 7: probability of positioning failure given a pair of biases $(b_{A/C+ground+obs,1}, b_{A/C+ground+obs,2})$ on 2 pseudo range measurements - control during taxi

From Figure 6, $b_{A/C+ground+obs,0}$ is a single multipath fault when $|b_{A/C+ground+obs,0}|$ is roughly above 5.5m. Note that P_{single} is slightly dissymmetric with respect to the ordinate axis because of the presence of nominal biases on the pseudo range measurements.

$b_{A/C+ground+obs,1}$ and $b_{A/C+ground+obs,2}$ are double multipath faults when the biases pair $(b_{A/C+ground+obs,1}, b_{A/C+ground+obs,2})$ is located on or outside from the blue quadrilateral plotted in Figure 8. Note that the pseudo range measurements affected by the biases pair are not the same for all pairs. This creates small discontinuities on the blue line shown in Figure 8.

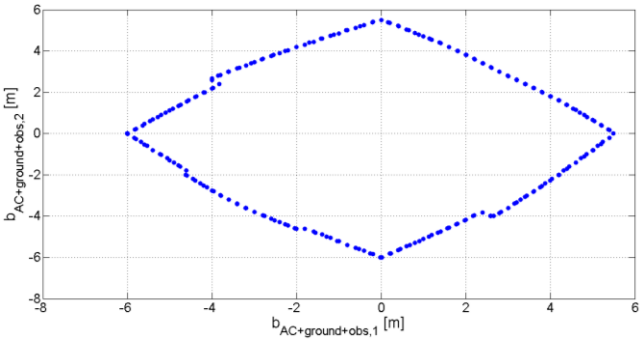

Figure 8: pairs of biases $(b_{A/C+ground+obs,1}, b_{A/C+ground+obs,2})$ that may lead to $P_{double} = 0.1 \times P_{IR}$ – control function during taxi

III.3.2.2. Dynamic case

The raw code ranging errors $\varepsilon_{code\ multipath}$ inconsistent with the nominal error distribution are errors due to multipath from the airport surface, the aircraft structure and obstacle(s). These errors are stochastic errors in the dynamic case and follow a Gaussian distribution characterized by a mean $b_{A/C+ground+obs}$ and a standard deviation $\sigma_{A/C+ground+obs}$. From Eq.14, multipath single fault in the dynamic case is a multipath ranging error characterized by a mean $b_{A/C+ground+obs}$ and a standard deviation $\sigma_{A/C+ground+obs}$ that may lead to:

$$P_{single} = P(|\varepsilon_{pos,hori}| > HAL \mid (b_{A/C+ground+obs}, \sigma_{A/C+ground+obs})) \geq 0.1 \times P_{IR} \quad \text{Eq.18}$$

Note that the identification of double multipath ranging faults for the dynamic case is not presented in this paper and is left as future work.

P_{single} is computed and plotted in Figure 9 for the control-taxi operation and in Figure 10 for the control- parking on the apron operation. In order to compute P_{single}, the same methodology as the one presented in Section **III.3.2.2** is used, knowing that $\boldsymbol{\varepsilon_{pos,hori}}$ is modeled by a 2 dimension Gaussian law proposed by Eq.7.

The probabilities of positioning failure presented in Figures 9 and 10 have been computed under the following conditions:

- The **selected satellites geometry** and **selected time instant** are detailed in Section **III.3.2.1**.
- The **pseudo range measurement** affected by the abnormal multipath error is selected in a way so as to maximize $P(|\varepsilon_{pos,hori}| > HAL \mid (b_{A/C+ground+obs}, \sigma_{A/C+ground+obs}))$.
-

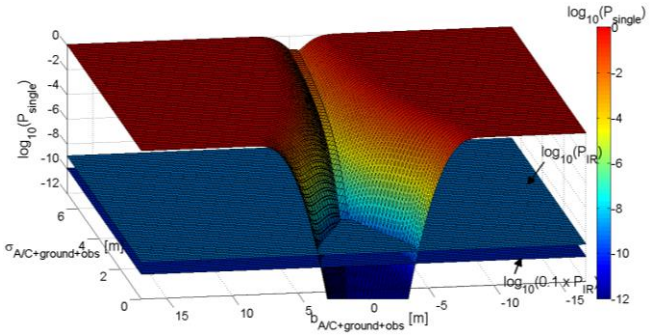

Figure 9: probability of positioning failure given a Gaussian ranging error $N(b_{A/C+ground+obs}, \sigma_{A/C+ground+obs})$ on a single pseudo range measurement – control during taxi

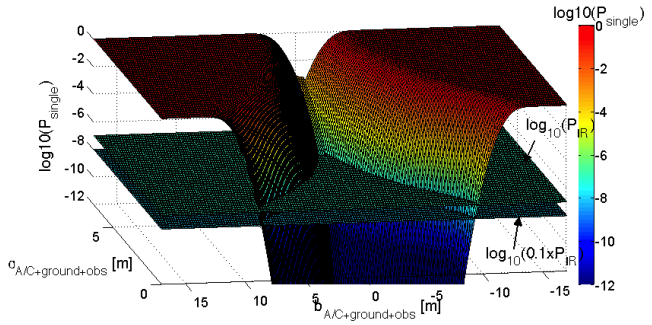

Figure 10: probability of positioning failure given a Gaussian ranging error $N(b_{A/C+ground+obs}, \sigma_{A/C+ground+obs})$ on a single pseudo range measurement – control during parking on the apron

The raw code ranging errors $\varepsilon_{code\ multipath}$ is a multipath fault when $(b_{A/C+ground+obs}, \sigma_{A/C+ground+obs})$ is located on or outside from the blue lines plotted in Figure 11 for the control -taxi operation and in Figure 12 for the control - parking on the apron operation.

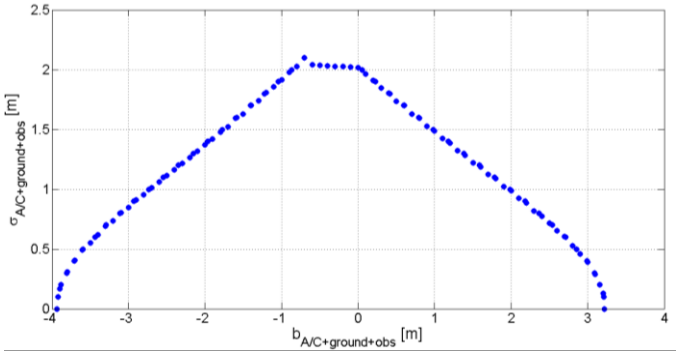

Figure 11: pairs $(b_{A/C+ground+obs}, \sigma_{A/C+ground+obs})$ that may lead to $P_{single} = 0.1 \times P_{IR}$ - control during taxi

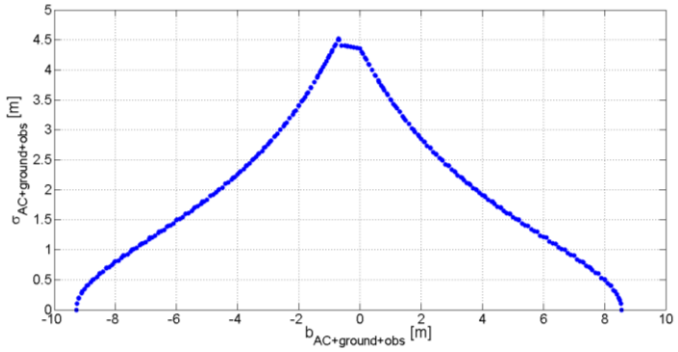

Figure 12: pairs $(b_{A/C+ground+obs}, \sigma_{A/C+ground+obs})$ that may lead to $P_{single} = 0.1 \times P_{IR}$ - control during parking on the apron

Note that P_{single} is slightly dissymmetric with respect to the ordinate axis because of the presence of nominal biases on the pseudo range measurements.
In addition, the performances of the positioning algorithm are slightly degraded in the dynamic configuration compared to the static configuration. For this reason, if we fix $\sigma_{A/C+ground+obs} = 0m$, biases $|b_{A/C+ground+obs}|$ above 4m are considered as faults in the dynamic case for control during taxi. In comparison, Section **III.3.2.1** shows that biases $|b_{A/C+ground+obs}|$ above 6m are considered as faults in the static case for control during taxi.
Finally, the HAL for the apron operation is almost twice the HAL for the taxi operation. This explains why some pairs (such as $(b_{A/C+ground+obs} = 6m, \sigma_{A/C+ground+obs} = 0.5m)$) are considered as faults for the taxi operation and not for the apron operation.

CONCLUSION AND FUTURE WORKS

In this paper, we have analyzed the impact of raw code ranging errors due to multipath from the aircraft structure, from the airport surface and from obstacles surrounding the airborne antenna on the horizontal position error in both static and dynamic configurations. Based on this analysis, we have identified which multipath ranging errors are considered as multipath faults. In the following, the obtained results are summarized and future works are proposed.

The impact of the multipath ranging errors in the horizontal positioning domain depends on the navigation algorithm used to estimate the aircraft position. Here we have considered a GNSS+INS tight coupling Kalman filter as navigation algorithm. In order to estimate the horizontal aircraft position, the Kalman filter hybridizes Galileo and GPS iono free measurements with the position, velocity and attitude angles estimated by the INS. Simulations show that this algorithm enables meeting the accuracy requirements of the control function for both taxi on the taxiway and parking on the apron operations.

After the selection of the navigation algorithm, the impact of the raw code multipath ranging errors on the horizontal position error has been analyzed. Multipath ranging errors are classified as follows. Ranging errors due to multipath from the airport surface and from the aircraft structure are considered as "nominal" errors. Ranging errors due to multipath from the airport surface, from the aircraft structure and from obstacles are considered as errors "inconsistent with the nominal error distribution", also called "abnormal" errors in this paper.
In the static case, nominal and abnormal multipath ranging errors are biases. In the horizontal positioning domain, these ranging biases induce 2-dimension (North

and East) deterministic horizontal position errors that converge to roughly constant values. Nominal multipath ranging biases lead to few cm deterministic positioning errors in the North and East directions. Abnormal multipath ranging biases of few m on one pseudo range measurement may occur in airport environments [4] and may lead to few dm deterministic positioning errors in the North and East directions. Abnormal multipath ranging biases combined with nominal ranging errors may lead to horizontal positioning errors larger than the HAL for the control function that is meter level.

In the dynamic case, nominal raw code multipath ranging errors remain bias errors while each abnormal multipath ranging error follows a stationary Gaussian distribution characterized by a mean $b_{A/C+ground+obs}$ and a standard deviation $\sigma_{A/C+ground+obs}$. In the horizontal positioning domain, $b_{A/C+ground+obs}$ are up to few m in airport environments [4] and induces 2-dimension (North and East) deterministic horizontal position errors that may reach few dm up to 1 meter. $\sigma_{A/C+ground+obs}$ induces an inflation of the covariance matrix of the horizontal position error. A multipath ranging error characterized by a standard deviation of few m on one pseudo range measurement may occur in airport environments [4] and may generate an increase of the standard deviation of positioning error in the North and East directions. More precisely, the standard deviation of the positioning error under nominal conditions is roughly 30cm and may be doubled in the presence of a stochastic multipath ranging error characterized with a standard deviation $\sigma_{A/C+ground+obs}$ of 3m. Finally, abnormal multipath errors influence both the deterministic positioning errors and variance of positioning errors. This may lead to horizontal positioning errors larger than the HAL for the control function that is meter level.

Based on the analysis of the impact of the multipath ranging errors on the horizontal position error, multipath faults have been identified. A multipath single fault has been defined as a raw code multipath ranging error that is inconsistent with the nominal distribution error and that may induce a horizontal position error larger than the HAL with a probability that is non-negligible with respect to the integrity risk. Similarly, multipath multiple faults are multiple abnormal multipath errors on multiple ranging measurements that may induce a horizontal position error larger than the HAL with a probability that is non-negligible with respect to the integrity risk. Hence, the multipath faults identification depends on the pair function/operation.

In the static case, and for the control function during taxi operations, simulations results show that:

- a single multipath fault is an abnormal ranging bias whose absolute value exceeds roughly 5.5m.
- a double multipath fault is a pair of abnormal ranging biases in a way so as the sum of the absolute value of each bias of the pair exceeds roughly 5.5m.

Since the aircraft is not likely to stop during parking on the apron operations, single faults modes during apron operations in static case have not been identified.

In the dynamic case, a single multipath faults are characterized by a mean $b_{A/C+ground+obs}$ and by a standard deviation $\sigma_{A/C+ground+obs}$ that have been identified for the control function during taxi operations and during parking on the apron operations. Simulations results show that:

- if $b_{A/C+ground+obs} = 0m$, the standard deviation $\sigma_{A/C+ground+obs}$ of single multipath faults exceeds 2m for the taxi operation and 4.4m for the apron operation.
- if $\sigma_{A/C+ground+obs} = 0m$, the absolute value of the mean $b_{A/C+ground+obs}$ of single multipath faults exceeds 3.2m for the taxi operation and 8.5m for the apron operation.

This paper proposes an identification of the single and double multipath faults for the static configuration. It also proposes an identification of the single multipath faults for the dynamic configuration. Future works can be organized as follows. The identification of double multipath faults for the dynamic configuration has to be performed. Next, probabilities of occurrence of multipath faults modes are required in order to define an algorithm that properly detect the multipath faults. An understanding of the environmental parameters that influence the occurrence of multipath faults along a trajectory in a given airport is necessary to derive probabilities of occurrence of multipath faults. Finally, the identification of multipath faults modes and probabilities of occurrence will represent a basis to develop an integrity monitoring capable to properly detect and exclude multipath faults.

APPENDIX

Let's assume that, during a surface operation, N GNSS pseudo range measurements are used in the Kalman filter to estimate the aircraft position. At time epoch t_l, each GNSS pseudo range measurement "sat j", $j \in [\![1, N]\!]$, is affected by:

- a pseudo range measurement error $v_{sat\,j,l}$ that is the sum of the ranging error resulting from the receiver noise, the ranging error resulting from the residual satellite clock error and from ephemeris errors, the ranging error resulting from the tropospheric delay estimation error.
- if $t_l \geq t_K$, a pseudo range measurement error $u_{sat\,j,l}$ that can be decomposed into:
    - A deterministic bias $b_{sat\,j,l}$,
    - A stochastic error $x_{sat\,j,l}$ modeled as a first-order Gauss-Markov process with an auto-correlation time $T_{sat\,j}$ and a standard deviation $\sigma_{sat\,j}$:

$$\begin{cases} x_{sat\,j,l} = \eta_{sat\,j,l} \text{ for } t_l = t_K \\ x_{sat\,j,l} = e^{-\frac{T_e}{T_{sat\,j}}} \times x_{sat\,j,l-1} + \eta_{sat\,j,l} \text{ for } t_l > t_K \end{cases}$$

where:

- T_e is the sampling period of the GNSS pseudo range measurement estimates,
- $\eta_{sat\,j,l}$ is the noise term normally distributed with a standard deviation of $\sigma_{sat\,j}$ for $t_l = t_K$ and $\sigma_{sat\,j}\sqrt{1 - e^{-\frac{2\times T_e}{T_{sat\,j}}}}$ for $t_l > t_K$.

Let's compute the deterministic error vector and the covariance of the positioning error at the Kalman filter output in the horizontal domain at time t_l $\boldsymbol{\varepsilon_{pos,hori,l}}$. An important remark is that, in the following, a model of the true behavior of the position error is proposed assuming a sub-optimal Kalman filter. In other words, the filter does not contain the exact model of the measurement process. Indeed, the Kalman gain is calculated using a measurement error covariance matrix that does not contain the model of multipath errors.

Let's note $\mathbf{X_l}$ the state vector at time t_l and $\widehat{\mathbf{X}}_\mathbf{l}^+$ the updated state vector estimated by the Kalman filter at time t_l. The first line of $\mathbf{X_l}$ represents the position error at time t_l in the Norh direction. The second component of $\mathbf{X_l}$ represents the position error at time t_l in the East direction:

$$\boldsymbol{\varepsilon_{pos,hori,l}} = \left(\mathbf{X_l} - \widehat{\mathbf{X}}_\mathbf{l}^+\right)_{1:2} \qquad \text{A.1}$$

The state vector at time t_l is given by the state propagation equation:

$$\mathbf{X_l} = \mathbf{F_{l-1}} \times \mathbf{X_{l-1}} + \boldsymbol{\omega_{l-1}} \qquad \text{A.2}$$

where:

- $\mathbf{F_{l-1}}$ is the state transition matrix from epoch t_{l-1} to t_l,
- $\boldsymbol{\omega_{l-1}}$ is the process noise vector at time t_{l-1}.

The updated state vector is obtained in the Kalman filter as follows:

$$\widehat{\mathbf{X}}_\mathbf{l}^+ = \widehat{\mathbf{X}}_\mathbf{l}^- + \mathbf{K_l} \times \left(\mathbf{Y_l} - \mathbf{H_l} \times \widehat{\mathbf{X}}_\mathbf{l}^-\right) \qquad \text{A.3}$$

where:

- $\mathbf{K_l}$ is the Kalman gain at time t_l,
- $\mathbf{H_l}$ is the design matrix at time t_l,
- $\mathbf{Y_l}$ is the measurement vector at time t_l, and is given by the observation model:

$$\mathbf{Y_l} = \mathbf{H_l} \times \mathbf{X_l} + \mathbf{v_l} + \mathbf{u_l} \qquad \text{A.4}$$

where:

- $\mathbf{v_l} = \begin{bmatrix} v_{sat\,1,l} \\ \vdots \\ v_{sat\,N,l} \end{bmatrix}$
- $\mathbf{u_l} = \begin{bmatrix} u_{sat\,1,l} \\ \vdots \\ u_{sat\,N,l} \end{bmatrix} = \begin{bmatrix} x_{sat\,1,l} \\ \vdots \\ x_{sat\,N,l} \end{bmatrix} + \begin{bmatrix} b_{sat\,1,l} \\ \vdots \\ b_{sat\,N,l} \end{bmatrix} = \mathbf{x_l} + \mathbf{b_l}$
- $\widehat{\mathbf{X}}_\mathbf{l}^-$ is the a priori state vector estimated by the Kalman filter at time t_l, and is obtained in the Kalman filter as:

$$\widehat{\mathbf{X}}_\mathbf{l}^- = \mathbf{F_{l-1}} \times \widehat{\mathbf{X}}_\mathbf{l-1}^+ \qquad \text{A.5}$$

Equations A.2, A.3, A.4, A.5 in A.1 lead to:

$$\mathbf{X_l} - \widehat{\mathbf{X}}_\mathbf{l}^+ = (\mathbf{I} - \mathbf{K_l} \times \mathbf{H_l})\left(\mathbf{F_{l-1}} \times \left(\mathbf{X_{l-1}} - \widehat{\mathbf{X}}_\mathbf{l-1}^+\right) + \boldsymbol{\omega_{l-1}}\right) - \mathbf{K_l} \times (\mathbf{v_l} + \mathbf{x_l} + \mathbf{b_l}) \qquad \text{A.6}$$

Esperance of $X_l - \widehat{X}_l^+$:

From Equation A.6:

$$\mathrm{E}\left[\mathbf{X_l} - \widehat{\mathbf{X}}_\mathbf{l}^+\right] = (\mathbf{I} - \mathbf{K_l} \times \mathbf{H_l})\left(\mathbf{F_{l-1}} \times \mathrm{E}\left[\mathbf{X_{l-1}} - \widehat{\mathbf{X}}_\mathbf{l-1}^+\right] + \mathrm{E}[\boldsymbol{\omega_{l-1}}]\right) - \mathbf{K_l} \times \mathrm{E}[\mathbf{v_l} + \mathbf{x_l} + \mathbf{b_l}] \qquad \text{A.7}$$

Assuming that the process noise vector is unbiased and remarking that $\mathrm{E}[\mathbf{v_l} + \mathbf{x_l} + \mathbf{b_l}] = \mathrm{E}[\mathbf{b_l}] = \mathbf{b_l}$ since the N elements of $\mathbf{v_l}$ and $\mathbf{x_l}$ are unbiased, Equation A.7 becomes:

$$\mathrm{E}\left[\mathbf{X_l} - \widehat{\mathbf{X}}_\mathbf{l}^+\right] = (\mathbf{I} - \mathbf{K_l} \times \mathbf{H_l})\left(\mathbf{F_{l-1}} \times \mathrm{E}\left[\mathbf{X_{l-1}} - \widehat{\mathbf{X}}_\mathbf{l-1}^+\right]\right) - \mathbf{K_l} \times \mathbf{b_l} \qquad \text{A.8}$$

where:

- $\mathrm{E}\left[\mathbf{X_0} - \widehat{\mathbf{X}}_\mathbf{0}^+\right] = \mathbf{0}$

To conclude we get:

$$\mathrm{E}\left[\boldsymbol{\varepsilon_{pos,hori,l}}\right] = \mathrm{E}\left[\mathbf{X_l} - \widehat{\mathbf{X}}_\mathbf{l}^+\right]_{1:2} \qquad \text{A.9}$$

$$\mathrm{E}[\boldsymbol{\varepsilon_{pos,hori,l}}] = \left((\mathbf{I} - \mathbf{K_l} \times \mathbf{H_l})\left(\mathbf{F_{l-1}} \times \mathrm{E}\left[\mathbf{X_{l-1}} - \widehat{\mathbf{X}}_\mathbf{l-1}^+\right]\right) - \mathbf{K_l} \times \mathbf{b_l}\right)_{1:2} \qquad \text{A.10}$$

where:

- $\mathrm{E}\left[\mathbf{X_0} - \widehat{\mathbf{X}}_\mathbf{0}^+\right] = \mathbf{0}$

Covariance of $X_l - \widehat{X}_l^+$:

It can be demonstrated by recurrence that:

$$\mathbf{X_l} - \widehat{\mathbf{X}}_\mathbf{l}^+ = \left(\mathbf{X_l} - \widehat{\mathbf{X}}_\mathbf{l,sat\&eph,tropo,noise}^+\right) + \Delta\mathbf{X_{l,mp}} \qquad \text{A.11}$$

where:

- $\mathbf{X_l} - \widehat{\mathbf{X}}_\mathbf{l,sat\&eph,tropo,noise}^+$ corresponds to the error in the estimation of the state vector if the measurement vector would have been $\mathbf{v_l}$,

- $\Delta\mathbf{X_{l,mp}} = (\mathbf{I} - \mathbf{K_l} \times \mathbf{H_l})(\mathbf{F_{l-1}} \times \Delta\mathbf{X_{l-1,mp}}) - \mathbf{K_l} \times (\mathbf{x_l} + \mathbf{b_l})$
- $\Delta\mathbf{X_{0,mp}} = \mathbf{0}$

Coming back to the computation of the covariance of $\mathbf{X_l} - \widehat{\mathbf{X}}_\mathbf{l}^+$, we have from Equation A.11:

$$\mathrm{cov}[\mathbf{X_l} - \widehat{\mathbf{X}}_\mathbf{l}^+] = \mathrm{cov}[(\mathbf{X_l} - \widehat{\mathbf{X}}^+_{\mathbf{l,sat\&eph,tropo,noise}}) + \Delta\mathbf{X_{l,mp}}] \quad \text{A.12}$$

Assuming that the noise process $\boldsymbol{\omega_l}$, the measurements errors vectors $\mathbf{x_l}$ and $\mathbf{v_l}$, and the error in the estimation of the state vector $\mathbf{X_l} - \widehat{\mathbf{X}}^+_{\mathbf{l,sat\&eph,tropo,noise}}$ are independent each other, we get:

$$\mathrm{cov}[\mathbf{X_l} - \widehat{\mathbf{X}}_\mathbf{l}^+] = \mathrm{cov}[(\mathbf{X_l} - \widehat{\mathbf{X}}^+_{\mathbf{l,sat\&eph,tropo,noise}})] + \mathrm{cov}[\Delta\mathbf{X_{l,mp}}] \quad \text{A.13}$$

Let's compute $\boldsymbol{cov[\Delta X_{l,mp}]}$***:***

$$\mathrm{cov}[\Delta\mathbf{X_{l,mp}}] = \mathrm{cov}[(\mathbf{F_{l-1}} - \mathbf{K_l} \times \mathbf{H_l} \times \mathbf{F_{l-1}})\Delta\mathbf{X_{l-1,mp}} - \mathbf{K_l} \times \mathbf{x_l}] \quad \text{A.14}$$

For $t_l \geq t_K$, $\mathbf{x_l}$ can be written as follows:

$$\mathbf{x_l} = \underbrace{\begin{bmatrix} e^{-\frac{T_e}{T_{sat\,1}}} & 0 & 0 \\ 0 & \ddots & 0 \\ 0 & 0 & e^{-\frac{T_e}{T_{sat\,N}}} \end{bmatrix}}_{\mathbf{CORR_l}} \times \underbrace{\begin{bmatrix} x_{sat\,1,l-1} \\ \vdots \\ x_{sat\,N,l-1} \end{bmatrix}}_{\mathbf{x_{l-1}}} + \underbrace{\begin{bmatrix} \eta_{sat\,1,l} \\ \vdots \\ \eta_{sat\,N,l} \end{bmatrix}}_{\boldsymbol{\eta_l}} \quad \text{A.15}$$

Hence:

$$\mathrm{cov}[\Delta\mathbf{X_{l,mp}}] = \mathrm{cov}[(\mathbf{F_{l-1}} - \mathbf{K_l} \times \mathbf{H_l} \times \mathbf{F_{l-1}})\Delta\mathbf{X_{l-1,mp}} - \mathbf{K_l} \times (\mathbf{CORR_l} \times \mathbf{x_{l-1}} + \boldsymbol{\eta_l})] \quad \text{A.16}$$

Since $\boldsymbol{\eta_l}$ is independent of $\Delta\mathbf{X_{l-1,mp}}$ and $\mathbf{x_{l-1}}$, A.16 is equivalent to:

$$\mathrm{cov}[\Delta\mathbf{X_{l,mp}}] = \mathrm{cov}[\mathbf{B_l} \times \Delta\mathbf{X_{l-1,mp}}] + \mathrm{cov}[\mathbf{K_l} \times \mathbf{CORR_l} \times \mathbf{x_{l-1}}] + \mathrm{cov}[\mathbf{K_l} \times \boldsymbol{\eta_l}] - 2\mathrm{cov}[\mathbf{B_l} \times \Delta\mathbf{X_{l-1,mp}}, \mathbf{K_l} \times \mathbf{CORR_l} \times \mathbf{x_{l-1}}] \quad \text{A.17}$$

where:

- $\mathbf{B_l} = \mathbf{F_{l-1}} - \mathbf{K_l} \times \mathbf{H_l} \times \mathbf{F_{l-1}}$

Equation A.17 is equivalent to:

$$\mathrm{cov}[\Delta\mathbf{X_{l,mp}}] = \mathbf{B_l}\mathrm{cov}[\Delta\mathbf{X_{l-1,mp}}]\mathbf{B_l}^\mathbf{T} + \mathbf{K_l} \times \mathrm{cov}[\mathbf{x_l}] \times \mathbf{K_l}^\mathbf{T} - 2\mathbf{B_l}\mathrm{E}[\Delta\mathbf{X_{l-1,mp}} \times \mathbf{x_{l-1}}^\mathbf{T}]\mathbf{CORR_l}^\mathbf{T}\mathbf{K_l}^\mathbf{T} \quad \text{A.17}$$

$\mathrm{E}[\Delta\mathbf{X_{l-1,mp}} \times \mathbf{x_{l-1}}^\mathbf{T}]$ can be computed by recurrence. Indeed, using Equations A.15 and A.11 we get:

$$\mathrm{E}[\Delta\mathbf{X_{l-1,mp}} \times \mathbf{x_{l-1}}^\mathbf{T}] = \mathbf{B_{l-1}}\mathrm{E}[\Delta\mathbf{X_{l-2,mp}} \times \mathbf{x_{l-2}}^\mathbf{T}]\mathbf{CORR_{l-1}}^\mathbf{T} - \mathbf{K_{l-1}} \times \mathrm{cov}[\mathbf{x_{l-1}}] \quad \text{A.18}$$

Finally we get:

$$\mathrm{cov}[\Delta\mathbf{X_{l,mp}}] = \mathbf{B_l}\mathrm{cov}[\Delta\mathbf{X_{l-1,mp}}]\mathbf{B_l}^\mathbf{T} + \mathbf{K_l} \times \mathbf{R_{mp,l}} \times \mathbf{K_l}^\mathbf{T} - 2\mathbf{B_l}\mathrm{E}[\Delta\mathbf{X_{l-1,mp}} \times \mathbf{x_{l-1}}^\mathbf{T}]\mathbf{CORR_l}^\mathbf{T}\mathbf{K_l}^\mathbf{T} \quad \text{A.19}$$

where:

- $\mathbf{B_l} = \mathbf{F_{l-1}} - \mathbf{K_l} \times \mathbf{H_l} \times \mathbf{F_{l-1}}$
- $\mathrm{E}[\Delta\mathbf{X_{0,mp}} \times \mathbf{x_0}^\mathbf{T}] = \mathbf{0}$
- $\mathrm{cov}[\Delta\mathbf{X_{0,mp}}] = \mathbf{0}$
- $\mathbf{R_{mp,l}} = \mathrm{cov}[\mathbf{x_l}]$
- $\mathbf{CORR_l} = \begin{bmatrix} e^{-\frac{T_e}{T_{sat\,1}}} & 0 & 0 \\ 0 & \ddots & 0 \\ 0 & 0 & e^{-\frac{T_e}{T_{sat\,N}}} \end{bmatrix}$

Let's compute $\boldsymbol{cov[(X_l - \widehat{X}^+_{l,sat\&eph,tropo,noise})]}$***:***

In order to remove the highest correlated pseudo range measurement error, that is to say the ranging error resulting from the residual satellite clock error and from ephemeris errors, the state-augmented algorithm detailed in [14] is implemented in the Kalman filter bloc illustrated in Figure 1.

With the state-augmented algorithm implementation, the covariance matrix of the positioning error due to $\mathbf{v_l}$ is denoted as $\mathbf{C_{l,sat\&eph,tropo,noise}}$. Note that, since the N GNSS satellites are considered as static during a surface operation, the standard deviations of the of pseudo range measurement errors are roughly constant during this time period. As a consequence, $\mathbf{C_{l,sat\&eph,tropo,noise}}$ remains roughly constant during a surface operation:

$$(\mathrm{cov}[(\mathbf{X_l} - \widehat{\mathbf{X}}^+_{\mathbf{l,sat\&eph,tropo,noise}})])_{1:2,1:2} = \mathbf{C_{sat\&eph,tropo,noise}} \quad \text{A.20}$$

Conclusion:

Finally the following result has been demonstrated:

$$\boldsymbol{\varepsilon}_{\mathbf{pos,hori,l}} \sim \mathrm{N}(\mathrm{E}[\boldsymbol{\varepsilon}_{\mathbf{pos,hori,l}}], \mathrm{cov}[\boldsymbol{\varepsilon}_{\mathbf{pos,hori,l}}]) \quad \text{A.21}$$

where:

- $\mathrm{E}[\boldsymbol{\varepsilon}_{\mathbf{pos,hori,l}}]$ is given by Equation A.10,
- $\mathrm{cov}[\boldsymbol{\varepsilon}_{\mathbf{pos,hori,l}}] = \mathbf{C_{sat\&eph,tropo,noise}} + \mathrm{cov}[\Delta\mathbf{X_{l,mp}}]_{1:2;1:2}$, $\mathrm{cov}[\Delta\mathbf{X_{l,mp}}]$ is given by Equation A.19.

REFERENCES

[1]: "A methodology to Elaborate Aircraft Localization Requirements for Airport Navigation", A. Guilloton, J.P. Arethens, C. Macabiau, A.C. Escher, D. Koenig, ION GNSS 2011

[2]: “Development of a GPS deterministic multipath simulator for a, efficient computation of the positioning errors”, A. Chen, A. Chabory, A-C Escher, C. Macabiau, 22nd International Meeting of the Satellite Division of The Institute of Navigation, September 2009

[3]: “Characterization of the Earth-Surface Multipath Error for Aircraft GPS Receivers”, Z. Zhu, F. van Graas, ION GNSS 18th International Technical Meeting of the Satellite Division, Long Beach, CA, September 2005

[4]: “GNSS Multipath Error Model for Surface Operations”, L. Montloin, L. Azoulai, A. Chen, A. Martineau, C. Milner, A. Chabory, C. Macabiau, ION GNSS 2012

[5]: “Study of the contribution of GNSS/UNS hybridization to GNSS integrity monitoring for civil aviation applications”, A.C. Escher, PhD dissertation, Université de Toulouse, December 2003

[6]: “Hybridisation of a GPS Receiver with Low-Cost Sensors for Personal Positioning in Urban Environment”, D. Kubrac, PhD dissertation, Ecole nationale supérieure des télécommunications de Paris, May 2007

[7]: “Annex 10 to the Convention on International Civil Aviation, Aeronautical Telecommunications, Volume I Radio Navigation Aids”, International Civil Aviation Organization, Sixth Edition, July 2006

[8]:”Minimum operational performance standards for Global Positioning System / Aircrafts Based Augmentation System airborne equipment”, RTCA-DO 316, April 2009

[9]: “Integrity prediction and monitoring of navigation systems, PhD dissertation”, P.B. Ober, 2003

[10]: “RAIM with multiple faults”, J.E. Angus, Journal of the Institute of Navigation, Vol. 53, No.4, Winter 2006

[11]: “Extended Theory of Early-Late Code Tracking for a Band limited GPS Receiver”, J. Betz, K. Kolodziejski, Journal of the Institute of Navigation, Vol.47, No.3, Fall 2003

[12]: “Minimum operational performance specification for airborne open service Galileo satellite receiving equipment, Appendix E Integrity monitoring, v3.0”, EUROCAE, December 2010

[13]: “Integrity monitoring applied to the reception of GNSS signals in urban environments”, C.D. Salós Andrés, Doctorat de l’université de Toulouse, PhD dissertation, July2012

[14]: “The practical approaches to Kalman filtering with time-correlated measurement errors”, K. Wang, Y. Li, C. Rizos, IEEE transactions on aerospace and electronic systems, VOL. 48, NO. April 2012

[15]: “ICAO-Manual on advanced surface movement guidance and control systems (A-SMGCS)”, Doc 9830 AN/452-First Edition 2004

[16]: “GPS integrity failure modes and effects analysis”, K. Van Dyke, K. Kovach, J. Lavrakas, JP. Fernow, J. Carroll, J. Kraemer, N. Attallah, B. Baevitz, ION NTM 2003

[17]: “The role of the Global Navigation Satellite System (GNSS) in supporting airport surface operations”, RTCA DO-247, January 1999